Available online at www.sciencedirect.com
ScienceDirect
Applied Surface Science 254 (2008) 2441–2449
applied surface science
www.elsevier.com/locate/apsusc

Analysis of XPS spectra of Fe^{2+} and Fe^{3+} ions in oxide materials

Toru Yamashita *, Peter Hayes

Pyrometallurgy Research Centre, School of Engineering, University of Queensland, Qld 4072, Australia

Received 25 September 2006; received in revised form 31 July 2007; accepted 21 September 2007
Available online 29 September 2007

Abstract

Samples of the iron oxides $Fe_{0.94}O$, Fe_3O_4, Fe_2O_3, and Fe_2SiO_4 were prepared by high temperature equilibration in controlled gas atmospheres. The samples were fractured in vacuum and high resolution XPS spectra of the fractured surfaces were measured. The peak positions and peak shape parameters of Fe 3p for Fe^{2+} and Fe^{3+} were derived from the Fe 3p XPS spectra of the standard samples of $2FeO{\cdot}SiO_2$ and Fe_2O_3, respectively. Using these parameters, the Fe 3p peaks of Fe_3O_4 and $Fe_{1-y}O$ are analysed. The results indicate that high resolution XPS techniques can be used to determine the Fe^{2+}/Fe^{3+} ratios in metal oxides. The technique has the potential for application to other transition metal oxide systems.

Keywords: XPS; Iron oxide; Quantitative analysis; Chemical state

1. Introduction

The chemical systems encountered in the high temperature smelting of non-ferrous metals are complex in that typically they

(i) contain many chemical species, some elements being present in a number of different oxidation states,
(ii) involve the coexistence of solid and liquid phases, and
(iii) the chemical species present in the system are partitioned between liquid metal alloy, and liquid and solid oxide phases.

The ability to control the partitioning of these elements between these phases is of crucial importance to the efficient operation of these metallurgical processes, since it allows the selective separation of chemical species into different process streams at the various stages of the operations. In industrial practice the variables used to control the chemical behaviour of the systems include, bulk composition of the slag, the oxygen partial pressure and the temperature.

The chemical behaviour of these complex systems can only be systematically analysed and understood when fundamental data on all species are incorporated into chemical thermodynamic models of the system. The transition metals possess the ability to exist in a number of different oxidation states in both solid and liquid oxides. For example, species, such as, as iron can be present as Fe^{2+} or Fe^{3+}; chromium as Cr^{2+}, Cr^{3+} or Cr^{6+}; manganese as Mn^{2+}, Mn^{3+} or Mn^{4+}; antimony as Sb^{2+} or Sb^{5+}; tin as Sn^{2+} or Sn^{4+}; titanium as Ti^{2+}, Ti^{3+} or Ti^{4+}; vanadium as V^{3+}, V^{4+} or V^{5+}.

X-ray photoelectron spectroscopy (XPS) is a versatile surface analysis technique that can be used for compositional and chemical states analysis. Since X-rays are used for the incident beam in XPS, the XPS technique causes very little charging of samples and thus it is useful for both electrically conductive and non-conductive materials. The attenuation length depends on the electron kinetic energy and emission angle [1]. For the electron energies that are normally used in XPS, the attenuation lengths are about 1–10 monolayers for the emission angles normal to the surface [1].

It has been shown in previous studies that the peak positions of Fe $2p_{1/2}$ and Fe $2p_{3/2}$ depend on the ionic states of Fe [2–7]. The positions of the satellite peaks for the Fe $2p_{1/2}$ and Fe $2p_{3/2}$ peaks are also very sensitive to the oxidation states and these peaks have been used for qualitatively determining the ionic states of iron.

Mekki et al. [6] used the Fe 3p spectra to obtain quantitative information on Fe^{2+} and Fe^{3+} concentrations in silicate glass samples. The Fe^{2+} and Fe^{3+} ions were assumed to generate overlapping Fe 3p spectra. These peaks were deconvoluted into

* Corresponding author. Present address: Microwave and Materials Designs Pty. Ltd., BTP Technology & Conference Centre, Clunies Ross Court, Eight Mile Plains, Qld 4113, Australia.
E-mail address: toru.yamashita@mandmd.com.au (T. Yamashita).
URL: http://pyrosearch.minmet.uq.edu.au

0169-4332/$ – see front matter © 2007 Elsevier B.V. All rights reserved.
doi:10.1016/j.apsusc.2007.09.063

two peaks to obtain the Fe^{2+} and Fe^{3+} ratios. Though this method is simple since no standard peak positions and FWHMs for Fe^{2+} and Fe^{3+} are determined, the validity of the method should be further investigated.

The quantitative analysis of the oxidation states of iron in the thin films has been carried out by Graat and Somers [3,4] using Tougaard's inelastic scattering theory. They measured the XPS Fe 2p spectra of the pure components Fe^0 from sputter-cleaned iron metal, Fe^{2+} from sputter-cleaned FeO powder and Fe^{3+} from Fe_2O_3 powder. By curve fitting the spectra of these standard samples, the principle parameters in Tougaard's formula were obtained. Using these parameters, the experimentally determined XPS spectra were analysed and the relative concentrations of Fe^{2+} and Fe^{3+} were estimated. However, the composition of their $Fe_{1-y}O$ is ambiguous in their work since wüstite is non-stoichiometric and is always Fe deficient at ambient pressures [8].

The aim of the present study is to develop a simple and easy to use methodology that enables quantitative analyses of Fe^{2+} and Fe^{3+} to be carried out on oxide samples using high resolution XPS of the Fe 3p peaks. Since the aim of this study is to develop a 'simple' method, the transmission function was not considered to be used for calculation. The proposed method would be valid when the same XPS apparatus is used to obtain measurements for both standards and unknown samples.

2. Experimental

An important first step in establishing a quantitative technique is the selection and preparation of standard materials. Particular attention has been paid to the preparation and characterisation of iron oxides through the control of oxygen partial pressure and temperature equilibration conditions.

X-ray powder diffraction (XRD) studies were undertaken to verify the phases present for all the samples. The XRD study was carried out using Bruker D8 Advance (Bruker AXS, Germany) with a graphite monochromator using Cu Kα radiation.

2.1. α-Fe_2O_3 (haematite)

The crystal structure of hematite may be approximated to a close packed hexagonal oxygen sub-lattice with trivalent iron ions distributed amongst two thirds of the octahedral interstices, resulting in the formation of a rhombohedral corundum structure [9]. Haematite is stoichiometric below approximately 1273 K [10]. Thus, the standard sample of Fe_2O_3, in which all the iron as present as Fe^{3+}, was prepared by equilibrating Fe metal foil (0.5–1 mm thick) in a Pt crucible at 1273 K for 200 h in air and then furnace cooled to room temperature.

2.2. $2FeO{\cdot}SiO_2$ (fayalite)

The iron in the compound $2FeO{\cdot}SiO_2$ is present only as Fe^{2+} ions and fayalite has a crystal structure consisting of SiO_4 tetrahedra linked together by O–Fe–O bonds. The Fe^{2+} ions are coordinated by six oxygen ions lying at the corners of a very nearly regular octahedron, so that the whole structure can be described as a packing together of tetrahedra and octahedra [11]. $2FeO{\cdot}SiO_2$ is a stoichiometric compound and melts congruently at 1481 K [12]. At sub-solidus conditions the presence of excess iron oxide a mixture of $2FeO{\cdot}SiO_2$ and $Fe_{1-y}O$ is formed. To avoid possible complications in the analysis of Fe^{2+} signals arising from the presence of iron in $Fe_{1-y}O$ and $2FeO{\cdot}SiO_2$, the samples were deliberately prepared by heating below the solidus with excess of SiO_2 at metallic iron saturation. In this event the only Fe^{2+} XPS signals are emitted from the material originating from Fe_2SiO_4.

The appropriate amounts of (>99.99%) Fe, Fe_2O_3 and SiO_2 powders to form stoichiometric Fe_2SiO_4 are calculated; then, extra 5% SiO_2 powder was added to the mixtures. The powders were thoroughly mixed with a mortar and pestle. The mixtures were pressed into discs and wrapped in the Fe foil and fired under flowing N_2 at 1473 K for 10 min followed by 1273 K for 3 h. The samples were furnace cooled down to room temperature over a period of 3 h.

2.3. Fe_3O_4 (magnetite)

Magnetite also consists of cubic close packed oxygen sub-lattice [9]. In the ideal crystal, the Fe^{2+} ions occupy the tetrahedral and the Fe^{3+} ions occupy the octahedral interstices forming a cubic spinel type structure. Although magnetite may exist over a range of compositions at high temperatures, at lower temperatures it approaches stoichiometric Fe_3O_4. Fe_3O_4 is alternatively expressed as $FeO{\cdot}Fe_2O_3$, i.e. the Fe^{2+}:Fe^{3+} atomic ratio is 1:2. To obtain the standard sample that has a composition close to the stoichiometric formula of Fe_3O_4 the oxygen partial pressure of 10^{-6} atm and the equilibration temperature of 1373 K were chosen as heat treatment conditions [10]. Iron metal strip (0.5–1 mm thick, 99.98% purity) (Aldrich Pty., Ltd.) was suspended by a Pt wire in a recrystallised alumina furnace tube (32 mm I.D.) and equilibrated at 1373 K in the flowing gas mixture of CO_2 (290.0 cc/min) and CO (2.2 cc/min). The sample was kept at the equilibration temperature for 166 h and then quenched into iced water.

2.4. $Fe_{1-y}O$ (wüstite)

The crystal structure of wüstite has a cubic lattice of the NaCl type, i.e. iron ions arranged in the octahedral interstices [9]. The oxygen sub-lattice is essentially fully occupied but a significant number of vacancies in Fe sites exist, indicating that the oxygen excess should be considered as an iron deficiency. Stoichiometric wüstite is not stable at atmospheric pressure [8]. The fraction of vacant iron ion lattice sites ranges from approximately 5 to 16 at% within the stable non-stoichiometric wüstite $Fe_{1-y}O$ phase field depending upon the activity of oxygen (oxygen gas partial pressure) and temperature; charge neutrality within the compound is maintained by the presence of both Fe^{3+} and Fe^{2+} ions. Oxide of controlled stoichiometry was prepared from iron metal strip (0.5–1 mm thick, 99.98% purity) (Aldrich Pty., Ltd.). The metal was suspended by a Pt

wire in a recrystallised alumina furnace tube (32 mm I.D.) and equilibrated at 1273 K in the flowing gas mixture of 35.5% CO_2 and 64.5% CO for 96 h. The sample was kept at the equilibration temperature for 50 h and then quenched into a beaker filled with high purity nitrogen gas at room temperature, this quenching medium was used to avoid potential oxidation of the sample during cooling.

The composition of the sample was determined through measurement of the lattice parameter of the non-stoichiometric $Fe_{1-y}O$. The XRD signal peak intensities and peak positions for $Fe_{1-y}O$ were analysed using the RIETAN-2000 computer program [13], for the Rietveld analysis. Commercially available high purity corundum Al_2O_3 powder was used as a standard sample for lattice parameter determinations. The XRD patterns of the sample was measured in the range of 10–120° in 2θ and the lattice parameters were obtained as the refined parameters of the Rietveld analysis.

2.5. XPS

XPS analyses were performed using KRATOS Axis Ultra (Kratos Analytical, Manchester, United Kingdom). An incident monochromated X-ray beam from the Al target (15 kV, 10 mA) was focused on a 0.7 mm × 0.3 mm area of the surface of the sample 45° to the sample surface. The electron energy analyser was operated with a pass energy of 20 eV enabling high resolution of the spectra to be obtained. The analyser is located perpendicular to the sample surface. The step size of 0.02 eV was employed and each peak was scanned twice.

This high surface sensitivity, although desirable, means that particular care is necessary in sample preparation since the sample surface can be easily contaminated. For example, the surfaces of most pure metals are readily oxidised in air [14]. To remove surface contamination the sputtering technique using Ar^+ ion bombardment is commonly employed. Though this sputtering method works well for the removal of loosely bound adsorbed species, in compounds preferential sputtering can occur [1]. A particular problem arises in the transition metals in which the metal can exist in a number of oxidation states. In the case of iron oxides, for example, Fe_2O_3 is reduced to Fe_3O_4 by Ar^+ sputtering in XPS analysis [15–17]. In these situations surface contamination and the effects of preferential sputtering are avoided by fracturing the sample under high vacuum prior to the XPS analysis without breaking vacuum [6]. All samples were fractured in high vacuum ($\sim 3 \times 10^{-8}$ Torr) in the Kratos outer pressure chamber before moving directly into the main XPS measurement chamber. The plate-like sample was notched from both sides and stand vertically on the sample holder (see Fig. 1(a and b)). The top of the sample was attached by carbon tape to an aluminium foil tape; the Al tape was fixed to the inner wall of the sample preparation chamber close to the sample insertion hatch. Then as the sample rod is inserted into the sample preparation chamber the sample is subjected to a bending force and fractured in the region of the notches. The XPS spectra were taken from up to six different locations on the fractured surface of the Fe_2O_3 standard sample in the measurement chamber (1×10^{-8} Torr).

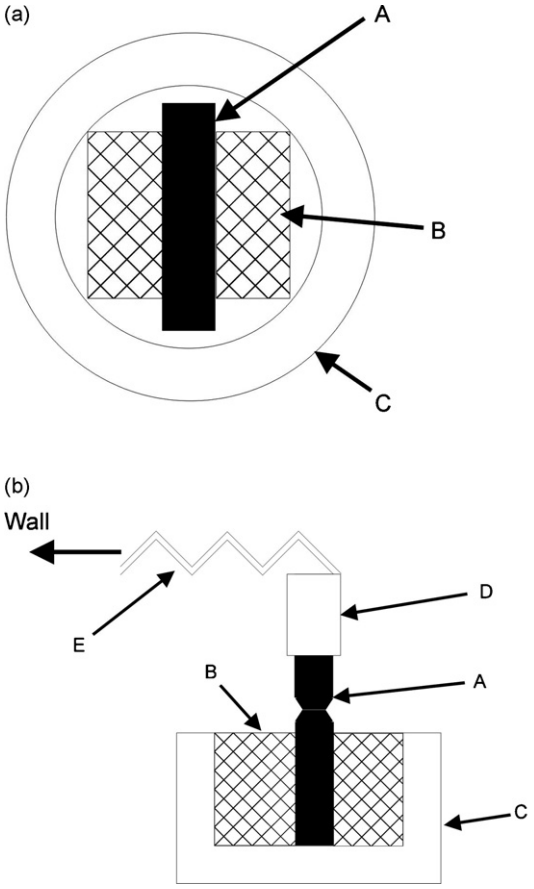

Fig. 1. (a) Top view and (b) side view of the sample in the sample holder. A: sample, B: Al block, C: sample holder, D: carbon tape, and E: Al foil (tape).

The details of curve fitting procedure are outlined in a previous publication by the authors [7]. Outline of the procedure is as follows. (1) Select the binding energy range for background subtraction. (2) Select the linear method for the background subtraction. (3) Select Gaussian–Lorentzian (GL) ratio (initial number is 0) to determine peak shape. (4) Select asymmetry factor (initial number is 1.0). (5) Select full width at half maximum (FWHM) for the specific peaks. (6) Select the best fitted curve for experimentally obtained Fe 3p, which gives the minimum chi square. These steps were repeated until the best chi squared was given. The curve fitting parameters, i.e. full width at half maximum, asymmetry factor, GL ratio, were manually input independent of the Kratos software algorithm. The peak shape was fitted to a Voigt function, which is a widely used, convenient means of mathematically describing the shape of the peak. The use of a single asymmetric Voigt function in the present study does not imply that the asymmetry arises from a single chemical species.

Carbon is ubiquitous and is present on all surfaces for XPS analysis. It is common practice to use the carbon C 1s peak at 285 eV as a reference for charge correction. In routine XPS analyses of samples prepared outside the high vacuum chamber relatively thick carbon layers are formed on the surfaces, and the corrected XPS peak positions are independent of the apparent or experimentally obtained binding energy. In Fig. 2(a) the Fe $2p_{3/2}$ peak positions in Fe_3O_4 corrected using

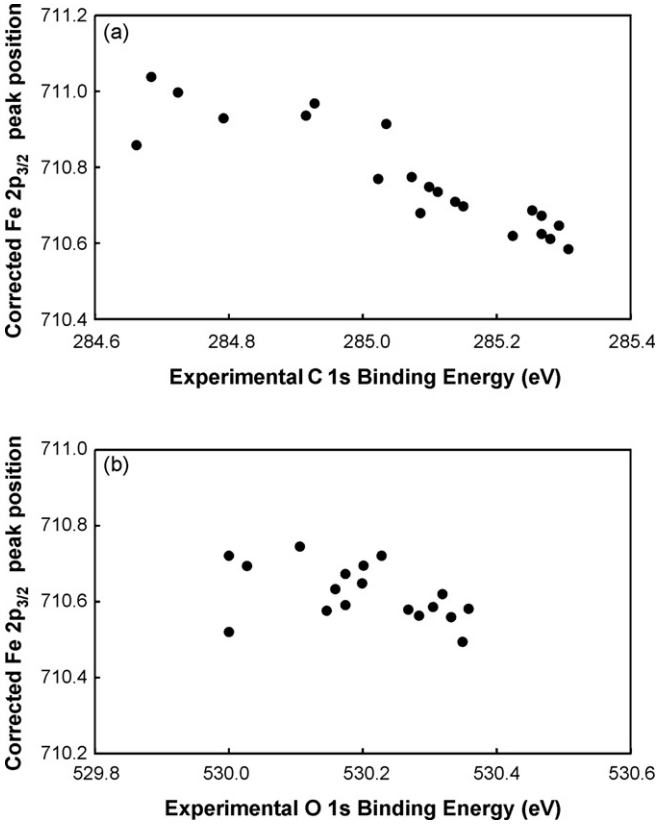

Fig. 2. (a) The Fe $2p_{3/2}$ peak positions corrected using the C 1s peaks in fractured surface of Fe_3O_4 as a function of the experimentally obtained C 1s peak positions used for the correction. (b) The Fe $2p_{3/2}$ peak positions corrected using the O 1s peaks in fractured surface of Fe_3O_4 as a function of the experimentally obtained O 1s peak positions used for the correction.

the C 1s peaks of hydrocarbon are plotted against the experimentally obtained carbon peak positions. Thus, if the C 1s peak is the ideal reference, only one Fe 2p3/2 peak position (e.g. 711 eV) should be obtained regardless to the C is binding energy in Fig. 2(a). However, it clearly shows that corrected Fe $2p_{3/2}$ position decreases with increasing experimentally obtained C peak position. The reason why the corrected C 1s position is a function of the experimentally obtained C 1s peak position is not clear. Therefore, it is concluded that the C 1s peak is not the suitable reference peak. Instead, the O 1s peak was used as the reference for the charge correction in the present study. The binding energy of Fe $2p_{3/2}$ peak for Fe_3O_4 corrected using O 1s peak is shown in Fig. 2(b) as a function of the experimentally obtained O 1s peak position. It shows the corrected Fe $2p_{3/2}$ peak position to be independent of experimentally obtained O 1s peak position within experimental uncertainties. Although a number of values of the O 1s peak position have been reported [15,16,18–20] there is no convincing evidence to show that there is any systematic change in O 1s peak position with site occupancy or oxidation state in these iron oxides. Some of the factors influencing peak position in these systems have been discussed by the authors [21]. Therefore, since C 1s peak is not suitable for charge correction the O 1s peak with the binding energy of 530.0 eV was used for the charge correction throughout this study. The typical O 1s peaks for Fe_2O_3 and Fe_3O_4 are, respectively, shown in Fig. 3(a and b).

3. Results and discussion

The XRD patterns from the ground samples of Fe_2O_3, Fe_2SiO_4, Fe_3O_4 and $Fe_{1-y}O$ are given in Fig. 4(a–d); Fig. 4(a, c and d) shows that each of these samples contains only a single phase, these being, Fe_2O_3, Fe_3O_4 and $Fe_{1-y}O$, respectively. The XRD patterns from Fe_2SiO_4 contain small diffraction peaks from SiO_2. As mentioned in Section 2.4, the sample was deliberately prepared with excess SiO_2 so the all Fe is in the form of Fe_2SiO_4, i.e. all Fe is in the Fe^{2+} state.

3.1. Fe_2O_3

Initial XPS measurements were carried out on the Fe 2p peaks of Fe_2O_3. The XPS peaks of Fe $2p_{3/2}$ and Fe $2p_{1/2}$ for the Fe_2O_3 standard sample are shown in Fig. 5. Of the two peaks Fe $2p_{3/2}$ peak is narrower and stronger than Fe $2p_{1/2}$ and the area of

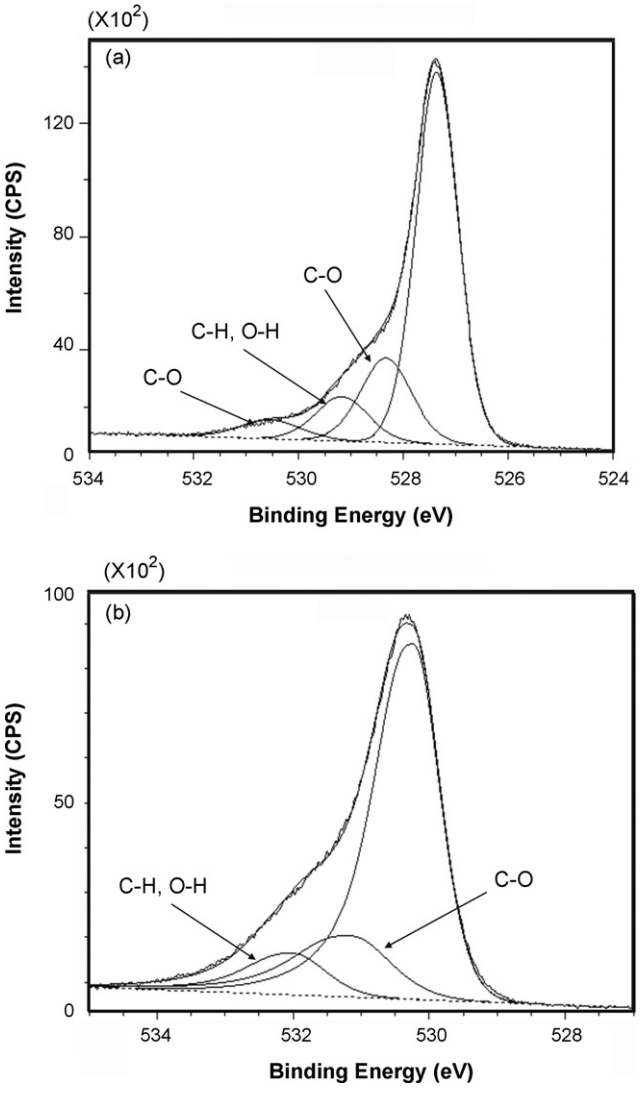

Fig. 3. The XPS spectra of O 1s from the fractured surfaces of the (a) Fe_2O_3 and (b) Fe_3O_4 standard samples.

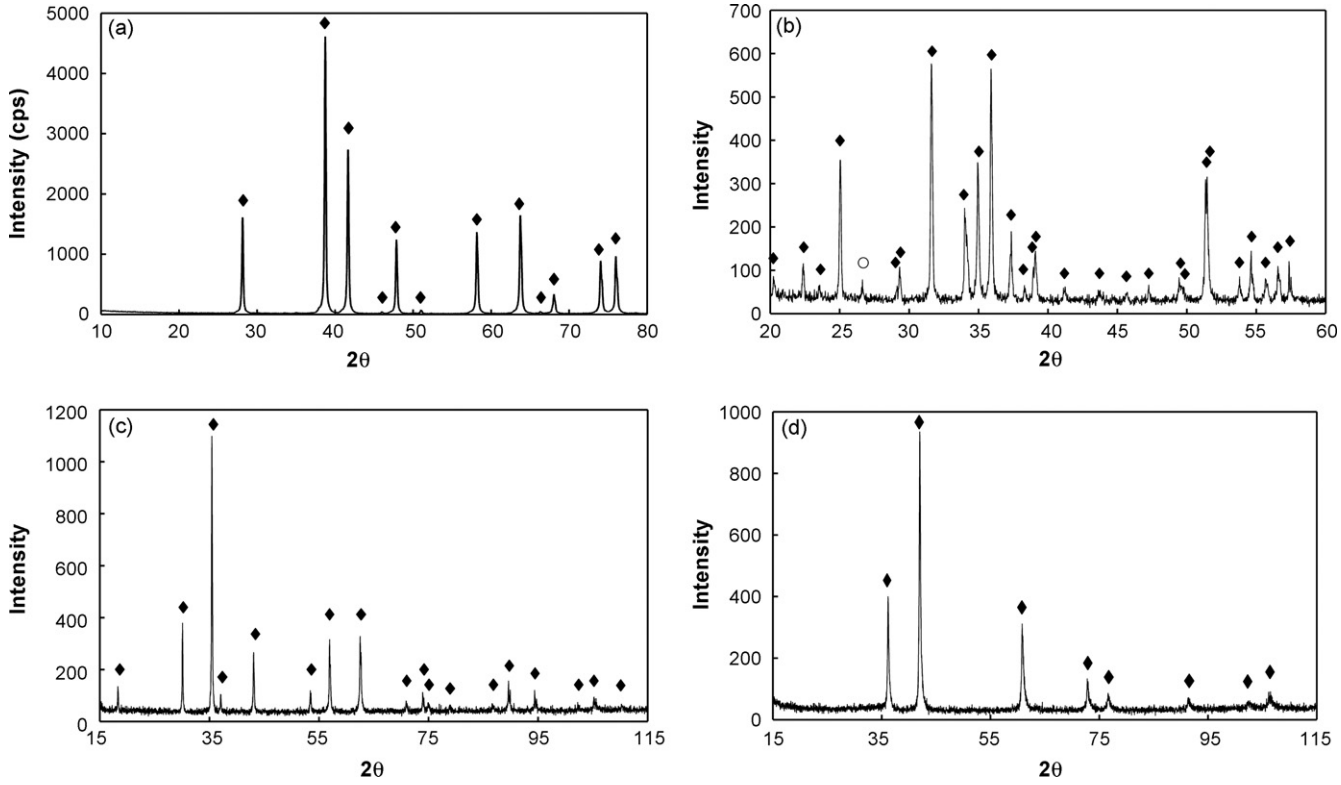

Fig. 4. XRD patterns of (a) Fe_2O_3, (b) Fe_2SiO_4, (c) Fe_3O_4 and (d) $Fe_{0.94}O$ powders (Cu Kα radiation). (◆) Indicates the diffraction peaks from the main phases and (○) indicates the peaks from the SiO_2 phase.

Fe $2p_{3/2}$ peak is greater than that of Fe $2p_{1/2}$ because in spin–orbit (j–j) coupling; Fe $2p_{3/2}$ has degeneracy of four states whilst Fe $2p_{1/2}$ has only two. The peak position of Fe $2p_{3/2}$ has been investigated by many researchers and the values of between 710.6 and 711.2 eV have been reported [2,3,17,22–24]. The Fe $2p_{3/2}$ peak has associated satellite peaks. The satellite peak of Fe $2p_{3/2}$ for Fe_2O_3 is located approximately 8 eV higher than the main Fe $2p_{3/2}$ peak [17,22,23]. The binding energies of Fe $2p_{3/2}$ and Fe $2p_{1/2}$ obtained from the present study are 711.0 (standard deviation (S.D.) = 0.01) and 724.6 eV (S.D. = 0.17), respectively. The satellite peak obtained at 718.8 (S.D. = 0.13) eV is clearly distinguishable and does not overlap either the Fe $2p_{3/2}$ or Fe $2p_{1/2}$ peaks. In addition, there appears to be another satellite peak at 729.5 eV; this may be a satellite peak for Fe $2p_{1/2}$.

The XPS spectrum of Fe 3p for the Fe_2O_3 standard sample is shown in Fig. 6. Although the Fe 3p peak consists of both Fe $3p_{3/2}$ and Fe $3p_{1/2}$, a single peak was observed in the XPS spectrum obtained from the present study. This separation energy of the XPS peaks is proportional to the spin–orbit coupling constant, which depends on the value $\langle 1/r^3 \rangle$ (where r is a radius) for the particular orbit [1]; thus the peak separation becomes smaller towards the outer shell. It would appear that the resolution of the current instrument although greater than in

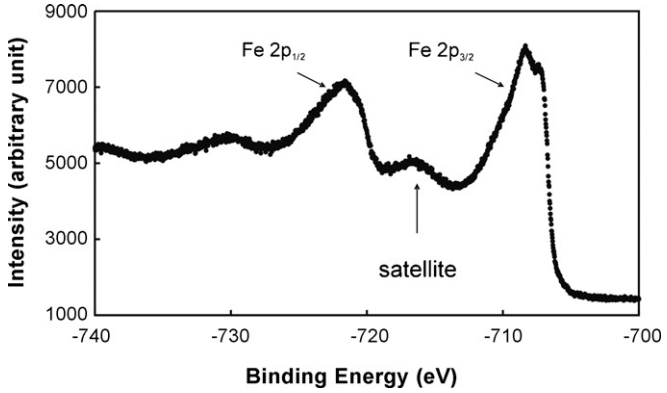

Fig. 5. The XPS spectrum of Fe 2p from the fractured surface of the Fe_2O_3 standard sample.

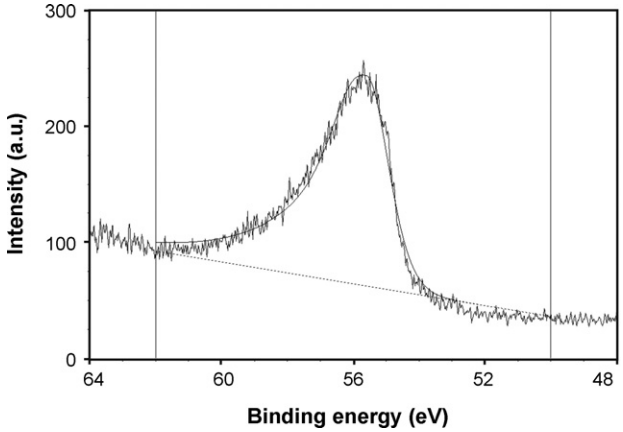

Fig. 6. The XPS spectrum of Fe 3p from the fractured surface of the Fe_2O_3 standard sample.

previous instruments cannot separate these two peaks at 3p level for Fe. Treating the Fe 3p peak as a single peak, the physical parameters, i.e. peak position, full width at half maximum, asymmetry factor and Gaussian–Lorentzian ratio of the Fe 3p peak for Fe^{3+} were determined from the spectrum. The curve fitting was carried out using the GL ratio = 40 (Gaussian:Lorentzian = 60:40), the symmetry factor of 0.4, and linear background subtraction between 62 and 50 eV which gave the smallest χ^2 [7]. The average values of the peak positions and the standard deviations of these parameters are listed in Table 1. The Fe 3p peak position for Fe^{3+} was found to be 55.6 eV (S.D. = 0.04) with FWHM of 3.1 eV (S.D. = 0.06).

3.2. $2FeO{\cdot}SiO_2$

The iron in the compound $2FeO{\cdot}SiO_2$ is only present as Fe^{2+} ions. The XPS spectra of Fe 2p and Fe 3p peaks for $2FeO{\cdot}SiO_2$ are shown in Figs. 7 and 8, respectively. The results of curve fitting with linear background subtraction between 62 and 50 eV give the Fe 3p peak position for $Fe^{2+}$of 53.7 eV (S.D. = 0.03) and FWHM of 3.7 eV (S.D. = 0.03) as shown in Table 1.

Table 1
Peak positions and FWHM of the XPS Fe 3p peak for Fe^{3+} obtained from Fe_2O_3 and for Fe^{2+} obtained from $2FeO{\cdot}SiO_2$. The table also shows the ratios of Fe^{2+} and Fe^{3+} for Fe_3O_4 and $Fe_{0.94}O$ using the peak positions and FWHMs obtained from $2FeO{\cdot}SiO_2$ and Fe_2O_3, respectively

	Peak position (eV)			Peak position (eV)		
	Fe 3p	FWHM	χ^2	Fe $2p_{1/2}$	Satellite	Fe $2p_{3/2}$
Fe^{3+} obtained from Fe_2O_3						
Fe_2O_3						
sample 1	55.6	3.2	2.77	724.4	718.8	711.0
sample 2	55.6	3.1	2.67	724.5	718.7	711.0
sample 3	55.5	3.1	2.42	724.8	718.9	711.0
average	55.6	3.1		724.6	718.8	711.0
S.D.	0.04	0.06		0.17	0.13	0.01
Fe^{2+} obtained from Fe_2SiO_4						
Fe_2SiO_4						
sample 1	53.8	3.7	2.76	722.6	714.7	709.0
sample 2	53.7	3.7	3.17	722.5	714.6	709.0
sample 3	53.7	3.7	3.19	722.6	714.8	708.9
sample 4	53.7	3.8	3.73	722.7	714.6	709.0
average	53.7	3.7		722.6	714.7	709.0
S.D.	0.03	0.03		0.05	0.11	0.02
	Atomic ratio			Peak position (eV)		
	Fe^{2+}	Fe^{3+}	χ^2	Fe $2p_{1/2}$	Satellite	Fe $2p_{3/2}$
Fe_3O_4						
Fe_3O_4						
sample 1	0.34	0.66	5.79	724.1		710.6
sample 2	0.34	0.66	9.19	724.1		710.6
sample 3	0.34	0.66	9.62	724.1		710.6
sample 4	0.36	0.64	4.49	724.0		710.5
average	0.35	0.65		724.07		710.56
S.D.	0.01	0.01		0.07		0.05
$Fe_{0.94}O$						
$Fe_{1-y}O$						
sample 1	0.72	0.28	7.59	723.1	715.5	709.5
sample 2	0.68	0.32	12.50	723.1	715.5	709.5
sample 3	0.72	0.28	7.50	723.2	715.5	709.5
sample 4	0.72	0.28	6.02	723.2	715.6	709.5
sample 5	0.69	0.31	7.43	723.2	715.5	709.5
sample 6	0.66	0.34	9.11	723.2	715.5	709.5
average	0.70	0.30		723.17	715.52	709.53
S.D.	0.03	0.03		0.05	0.05	0.02

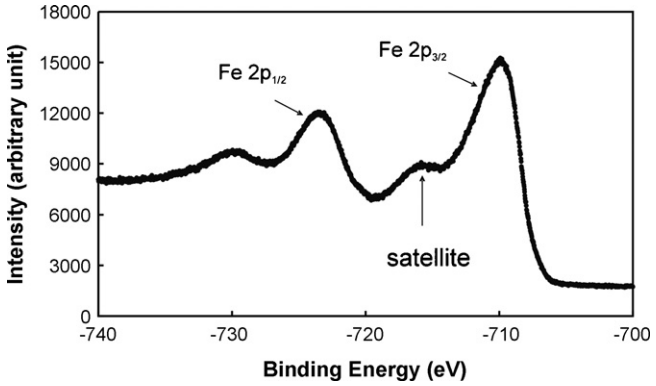

Fig. 7. The XPS spectrum of Fe 2p from the fractured surface of the Fe_2SiO_4 standard sample.

The peak width (FWHM), ΔE, is described as follows [1].

$$\Delta E = (\Delta E_n^2 + \Delta E_p^2 + \Delta E_a^2)^{1/2} \quad (1)$$

where ΔE_n is the inherent width of the core level, ΔE_p is the width of the X-ray line and ΔE_a is the analyser resolution. Since all the data were taken under the same conditions, ΔE_p and ΔE_a are considered constant for all peaks in the present study. The inherent line width of a core level is a direct reflection of uncertainty in the lifetime of the ion state remaining after photoemission and the line width is inversely proportional to the lifetime of the ion state remaining after photoemission [1]. The electronic configuration of Fe^{2+} is $3d^6$ whilst that of Fe^{3+} is $3d^5$. It means that Fe^{2+} will have a longer life time compared to Fe^{3+}; and it follows therefore that the FWHM of the Fe^{2+} peak is expected to be slightly smaller than the Fe^{3+} peak. As shown in Figs. 5 and 7, the FWHM of the Fe 2p peaks for Fe^{2+} is smaller than Fe^{3+}. On the other hand, it is observed that the FWHM of Fe 3p for Fe^{2+} is larger than Fe^{3+}. It is not clear why this should be the case.

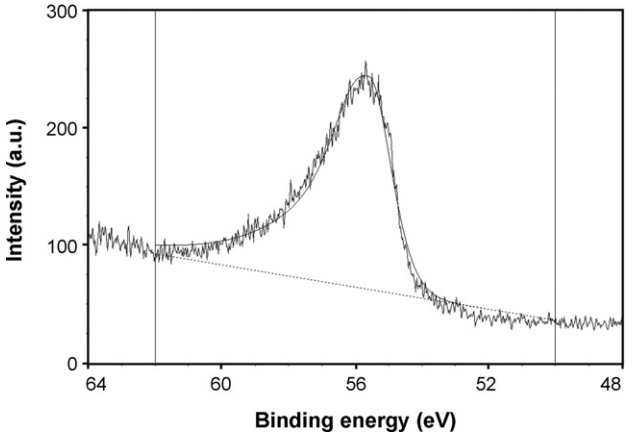

Fig. 8. The XPS spectrum of Fe 3p from the fractured surface of the Fe_2SiO_4 standard sample.

There are several reasons why Fe 3p peaks are used in the present study for the quantitative analysis of Fe^{3+} and Fe^{2+}. (1) The 2p peaks are separated into two peaks and to obtain the total contributions the intensities of both contributions have to be integrated, (2) the 2p peaks have satellite peaks that may partially overlap the main peaks depending on the oxidation states, (3) the base intensities of Fe $2p_{1/2}$ and Fe $2p_{3/2}$ are significantly different and appear to vary in a non-linear way with binding energy; it is not therefore possible to accurately subtract the background signal, and (4) the Fe 3p peak is a single peak without any interfering satellite peaks.

3.3. Fe_3O_4

It has been previously reported that Fe $2p_{3/2}$ for Fe_3O_4 does not have a satellite peak [22,23]. The absence of the satellite peak has been confirmed in the present study (Fig. 9). The peak positions of Fe $2p_{3/2}$ and Fe $2p_{1/2}$ are, respectively, 710.6 (S.D. = 0.05) and 724.1 eV (S.D. = 0.07) and they are located between the values obtained for $2FeO{\cdot}SiO_2$ and Fe_2O_3. The XPS spectrum of Fe 3p for Fe_3O_4 is shown in Fig. 10. Using the peak shape parameters and peak positions of Fe^{2+} and Fe^{3+} that are obtained from the present study on $2FeO{\cdot}SiO_2$ and Fe_2O_3, the Fe 3p peak for Fe_3O_4 was deconvoluted into the Fe^{2+} and Fe^{3+} peaks. The mean relative areas of each constituent peak assigned to Fe^{2+} and Fe^{3+} were calculated, these values and the standard deviations are listed in Table 1. Since stoichiometric Fe_3O_4 can also be expressed to $FeO{\cdot}Fe_2O_3$, the Fe^{2+}:Fe^{3+} ratio should be 1:2 or 0.33:0.67. The results of the deconvoluted peaks using the parameters defined above give Fe^{2+}:Fe^{3+} = 0.35:0.65; this value is clearly that of the stoichiometric oxide within the uncertainty of the calculations (S.D. = 0.01 for both Fe^{2+}:Fe^{3+}).

3.4. $Fe_{0.94}O$

The wüstite unit cell size of the sample was found from analysis of the XRD patterns to be 4.2903 Å and this value corresponds to $y = 0.082$–0.088 in $Fe_{1-y}O$ [10]. This compares with the value of $y = 0.06$ predicted from the gas composition and equilibration temperature [8]. The XPS spectrum of Fe 2p for $Fe_{1-y}O$ is shown in Fig. 11. The binding energies of Fe $2p_{3/2}$ and Fe $2p_{1/2}$ for the $Fe_{0.94}O$ standard sample are 709.5 (S.D. = 0.02) and 723.2 eV (S.D. = 0.05), respectively. The satellite peak for Fe $2p_{3/2}$ was observed at 715.5 (S.D. = 0.05). The binding energy difference between the Fe $2p_{3/2}$ peak and the satellite peak is approximately 6 eV. The presence of this 'shoulder' satellite peak and the binding energy difference of 6 eV are consistent with the results obtained by other researchers [2,3,17,23], and is clear evidence of the existence of Fe^{2+}.

The XPS spectrum of Fe 3p for $Fe_{1-y}O$ is shown in Fig. 12. Using the Fe^{2+} parameters that are obtained from the present study on $2FeO{\cdot}SiO_2$, $Fe_{1-y}O$ is analysed quantitatively and listed in Table 1. The ratio of Fe^{2+}:Fe^{3+} = 0.70:0.30 with a S.D. of 0.025 is obtained. Since $Fe_{1-y}O$ can be expressed as $2yFe^{3+}(1-3y)Fe^{2+}O$, the $Fe_{1-y}O$ that has the ionic ratio of Fe^{2+}:Fe^{3+} = 0.70:0.30 should have the composition of $Fe_{0.87}O$. This stoichiometry is different from the stoichiometry determined from the lattice parameter ($Fe_{1-y}O$ with $y = 0.082$–0.088) and also from the stoichiometry expected from the CO/CO_2 gas composition during the sample preparation ($Fe_{1-y}O$ with $y = 0.06$). This discrepancy appears likely to be the result of oxidation of the surface even in high vacuum. Wüstite is thermodynamically unstable below 590 °C

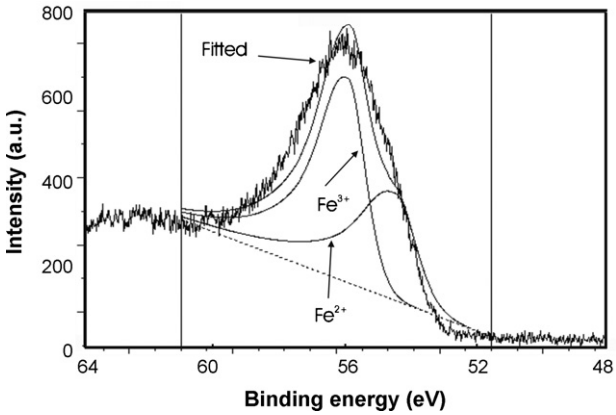

Fig. 10. The XPS spectrum of Fe 3p from the fractured surface of the Fe_3O_4 standard sample. The area between the thin vertical lines is chosen for background subtraction.

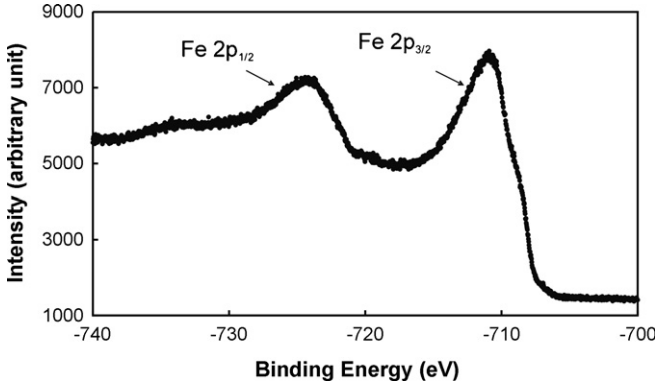

Fig. 9. The XPS spectrum of Fe 2p from the fractured surface of the Fe_3O_4 standard sample.

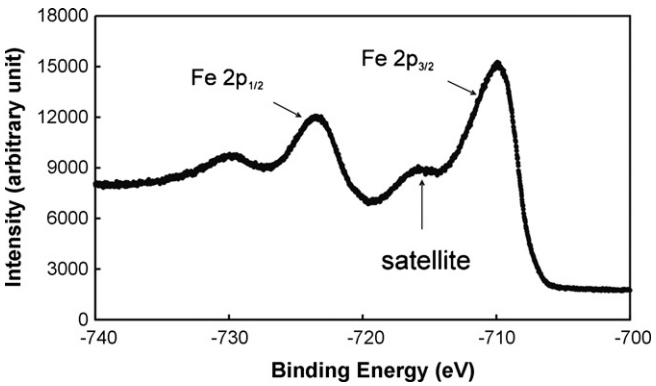

Fig. 11. The XPS spectrum of Fe 2p from the fractured surface of the $Fe_{0.96}O$ standard sample.

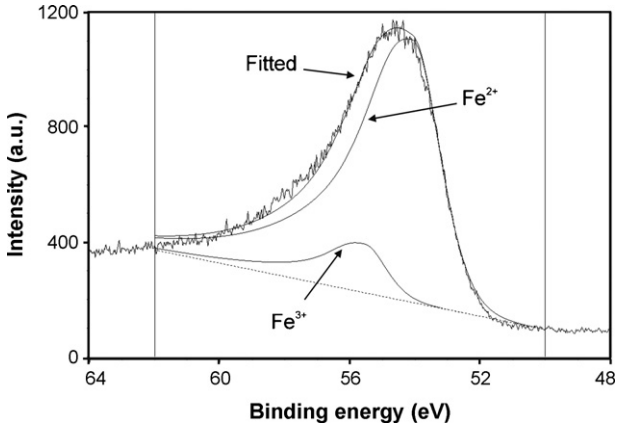

Fig. 12. The XPS spectrum of Fe 3p from the fractured surface of the $Fe_{0.96}O$ standard sample. The area between the thin vertical lines is chosen for background subtraction.

and it appears that, despite fracture under high vacuum conditions (1×10^{-8} Torr) the surface layers of this oxide become progressively oxidised, leading to changes in the stoichiometry of the oxide. This is an important finding since it demonstrates that wüstite, even prepared under high vacuum or ion beam cleaned conditions, is not suitable as a standard for the Fe^{2+} signal. Fayalite, $2FeO{\cdot}SiO_4$ appears to be a suitable, stable standard for Fe^{2+} measurement.

3.5. Application of the technique

The results of the present study have shown that through systematic analysis of the XPS spectra the proportions of Fe^{3+} and Fe^{2+} can be determined. The development of this methodology has potential applications to a range of oxides in which transition metals are present, e.g. glasses, complex stoichiometric compounds, in which the oxidation states of the individual metals cannot be determined by conventional analytical techniques. These oxide systems involve essentially close-packed arrangements of oxygen ions, with the metal ions occupying interstitial positions. This structural similarity can be seen in many transition metal oxides. For examples, the binding energies of Ti 3p are 36.0 and 37.5 eV for Ti^{3+} and Ti^{4+}, respectively [25,26], those of Mn 3p are 49.5 and 50.2 eV for Mn^{3+} and Mn^{4+} [27] and those of Co 3p are 60.2 and 61.1 eV for Co^{2+} and Co^{3+} [28]. Therefore, the method to determine Fe^{2+} and Fe^{3+} atomic ratios developed in this study may be applicable to other transition metal oxides systems.

4. Summary

The standard samples of high purity Fe_2O_3, $Fe_{0.94}O$, Fe_3O_4 and Fe_2SiO_4 have been prepared by heat treatment in controlled atmospheres. The XPS spectra obtained for Fe 2p for these samples show good agreement with previous studies, i.e. the satellite peak of Fe $2p_{3/2}$ for Fe^{2+} is a 'shoulder' peak of the Fe $2p_{3/2}$ peak whereas that for Fe^{3+} is a distinct peak.

The focus of the present work has been to determine the Fe^{2+}/Fe^{3+} atomic ratios in these oxides using the Fe 3p XPS peak. It has been shown that the best curve fit for Fe 3p for Fe^{3+} in Fe_2O_3 is obtained using the following curve fit parameters:

(1) linear background subtraction between 62 and 50 eV in binding energy;
(2) asymmetry factor of 0.4;
(3) 60% Gaussian–40% Lorentzian ratio.

The results of this curve fit give the Fe 3p peak position of 55.6 eV and FWHM of 3.1 eV for Fe^{3+}.

The curve fit for the Fe 3p peak for Fe^{2+} in $2FeO{\cdot}SiO_2$ gives the peak position of 53.7 eV and FWHM of 3.7 eV.

The XPS spectra of Fe 3p for Fe_3O_4, and $Fe_{0.94}O$ are analysed using the Fe^{3+} and Fe^{2+} peak parameters obtained from Fe_2O_3 and $2FeO{\cdot}SiO_2$. The results of the analyses show that the Fe^{2+}/Fe^{3+} atomic ratio in stoichiometric Fe_3O_4 is accurately predicted within experimental uncertainty. Wüstite, however, appears to be unstable even under high vacuum conditions, the measurements indicating partial oxidation of the surface. Solid wüstite even when prepared under controlled temperatures and oxygen partial pressures appears to be unsuitable as a standard material for Fe^{2+} measurements.

It has been shown in the present study that the proportions of iron present in different oxidation states can be determined using high resolution XPS measurements. There is an opportunity to extend this methodology to applications involving other transition metals to determine the relative concentrations of these ions in complex oxides, such as, complex oxide solid solutions, glasses and metallurgical slags.

Acknowledgements

The authors wish to thank Barry Wood, Brisbane Surface Analysis Centre, University of Queensland and Dr. Bill Bin Gong, School of Chemical Science, University of New South Wales, Sydney for their advice and assistance with this project and for the use of their respective research facilities.

This project was undertaken with funding from the Australian Research Council, Discovery program, Commonwealth of Australia.

References

[1] D. Briggs, M.P. Seah, Practical Surface Analysis, John Wiley & Sons Ltd., 1990.
[2] S.J. Roosendaal, B. van Asselen, J.W. Elsenaar, A.M. Vredenberg, F.H.P.M. Habraken, Surf. Sci. 442 (1999) 329.
[3] P.C.J. Graat, M.A.J. Somers, Appl. Surf. Sci. 100 (1996) 36.
[4] P.C.J. Graat, M.A.J. Somers, Surf. Interface Anal. 26 (1998) 773.
[5] C. Ruby, B. Humbert, J. Fusy, Surf. Interface Anal. 29 (2000) 377.
[6] A. Mekki, D. Holland, C.F. McConville, M. Salim, J. Non-Cryst. Solids 208 (1996) 267.
[7] T. Yamashita, P. Hayes, J. Electron Spectrosc. Relat. Phenom. 152 (2006) 6.
[8] A. Muan, E.F. Osborn, Phase Equilibria Among Oxides in Steelmaking, Addison-Wesley Pub. Co., 1965.
[9] F.S. Galasso, Structure and Properties of Inorganic Solids, Pergamon Press, 1970.
[10] L. von Bogdandy, H.-J. Engell, The Reduction of Iron Ores, Springer-Verlag, Berlin, 1971.

[11] R.C. Evans, An Introduction to Crystal Chemistry, second ed., Cambridge University Press, 1966.
[12] Slag Atlas, ed. Verein Deutscher Eisenhuttenleute, publ. Verlag Stahleisen, ISBN 3-514-00457-9, 2nd Ed, 1995.
[13] F. Izumi, T. Ikeda, Mater. Sci. Forum 198 (2000) 321.
[14] K. Wandelt, Surf. Sci. Rep. 2 (1982) 1.
[15] E. Paparazzo, Appl. Surf. Sci. 25 (1986) 1.
[16] R.J. Lad, V.E. Henrich, Surf. Sci. 193 (1988) 81.
[17] P. Mills, J.L. Sullivan, J. Phys. D: Appl. Phys. 16 (1983) 723.
[18] C.R. Brundle, T.J. Chuang, K. Wandelt, Surf. Sci. 68 (1977) 459.
[19] E. Paparazzo, J. Electron Spectrosc. Relat. Phenom. 43 (1987) 97.
[20] G.C. Allen, P.M. Tucker, R.K. Wild, Philos. Mag. B 46 (1982) 411.
[21] T. Yamashita, P. Hayes, J. Electron Spectrosc. Relat. Phenom. 154 (2006) 41.
[22] D.D. Hawn, B.M. DeKoven, Surf. Interface Anal. 10 (1987) 63.
[23] M. Muhler, R. Schlögl, G. Ertl, J. Catal. 138 (1992) 413.
[24] C.D. Wagner, L.H. Gale, R.H. Raymond, Anal. Chem. 51 (1979) 466.
[25] F. Werfel, O. Brummer, Phys. Scripta 28 (1983) 92.
[26] J. Riga, C. Tenret-Noel, J.J. Pireaux, R. Caudano, J.J. Verbist, Gobillon, Phys. Scripta 16 (1977) 35.
[27] G.C. Allen, S.J. Harris, J.A. Jutson, J.M. Dyke, Appl. Surf. Sci. 37 (1989) 111.
[28] N.S. McIntyre, M.G. Cook, Anal. Chem. 47 (1975) 2208.